Loss of muscle-specific RING-finger 3 predisposes the heart to cardiac rupture after myocardial infarction

Jens Fielitz*, Eva van Rooij*, Jeffrey A. Spencer*, John M. Shelton†, Shuaib Latif†, Roel van der Nagel‡, Svetlana Bezprozvannaya*, Leon de Windt‡, James A. Richardson*§, Rhonda Bassel-Duby*, and Eric N. Olson*¶

Departments of *Molecular Biology, †Internal Medicine, and §Pathology, University of Texas Southwestern Medical Center, 5323 Harry Hines Boulevard, Dallas, TX 75390-9148; and ‡Hubrecht Laboratory and Interuniversity Cardiology Institute, 3584 CT, Utrecht, The Netherlands

Contributed by Eric N. Olson, January 5, 2007 (sent for review December 26, 2006)

RING-finger proteins commonly function as ubiquitin ligases that mediate protein degradation by the ubiquitin-proteasome pathway. Muscle-specific RING-finger (MuRF) proteins are striated muscle-restricted components of the sarcomere that are thought to possess ubiquitin ligase activity. We show that mice lacking MuRF3 display normal cardiac function but are prone to cardiac rupture after acute myocardial infarction. Cardiac rupture is preceded by left ventricular dilation and a severe decrease in cardiac contractility accompanied by myocyte degeneration. Yeast two-hybrid assays revealed four-and-a-half LIM domain (FHL2) and γ-filamin proteins as MuRF3 interaction partners, and biochemical analyses showed these proteins to be targets for degradation by MuRF3. Accordingly, FHL2 and γ-filamin accumulated to abnormal levels in the hearts of mice lacking MuRF3. These findings reveal an important role of MuRF3 in maintaining cardiac integrity and function after acute myocardial infarction and suggest that turnover of FHL2 and γ-filamin contributes to this cardioprotective function of MuRF3.

heart failure | cardiac stress response | protein degradation | sarcomere

Maintenance of cardiac structure and function requires precise control of protein synthesis, processing, and degradation. Recent studies have shown that abnormalities in these processes result in lethal cardiomyopathies due to myofibrillar degeneration and contractile failure (reviewed in ref. 1).

The ubiquitin proteasome system (UPS) is largely responsible for the degradation of misfolded proteins, as well as long-lived proteins, such as components of the contractile apparatus of striated muscles (2). Although activation of the UPS in heart and skeletal muscle has been primarily linked to a reduction in muscle mass as occurs during muscle atrophy (3, 4), recent evidence has also shown the UPS to be activated during cardiac stress leading to hypertrophy and adverse cardiac remodeling (5). These apparently opposing functions of the UPS in striated muscles are poorly understood.

The substrate specificity of the ubiquitin conjugation cascade is mediated by hundreds of E3 ubiquitin protein ligases, which can be divided into three groups, RING-finger, HECT (homologous to E6AP carboxyl terminus)-domain, and SCF (Skp1-Cul1-F-box protein)-complex E3 ligases (6). Muscle-specific RING-finger (MuRF) proteins MuRF1, -2, and -3 comprise a subfamily of the RING-finger E3 ubiquitin ligases that are expressed specifically in cardiac and skeletal muscle (7). MuRF3, the first member of this family to be identified, associates with microtubules and is required for skeletal myoblast differentiation and development of cellular microtubular networks (7). MuRF1 is up-regulated during skeletal muscle atrophy, and mice lacking MuRF1 are resistant to skeletal muscle atrophy (8). No loss-of-function cardiac phenotypes of any of the three *MuRF* genes have yet been described.

The specific interaction partners of individual MuRF proteins and the consequences of such interactions are only beginning to be determined. MuRF1 and -2 interact with titin, nebulin, troponin I and T, myotilin, and T-cap in yeast two-hybrid assays (9); however, it remains to be determined whether all of these associated proteins serve as E3 ubiquitin ligase substrates. MuRF1 associates with titin at the M-band of the sarcomere that has been proposed to maintain stability of the sarcomeric M-line region (10, 11). MuRF2 binds to the titin kinase domain and is implicated in the serum response factor signal transduction pathway (12). MuRF1 was recently reported to function as an E3 ubiquitin ligase that catalyzes the ubiquitination and degradation of troponin I in cardiomyocytes (13). To date, no definitive substrates have been identified for MuRF3.

In the present study, we generated *MuRF3* mutant mice and showed that the absence of MuRF3 renders the heart highly susceptible to rupture after acute myocardial infarction (MI). Mice lacking MuRF3 display abnormal sarcomere structure, consistent with the localization of MuRF3 to the M-line and Z-disk. We show that MuRF3 interacts with Four-and-a-half LIM domain protein (FHL2) and γ-filamin. Accordingly, overexpression of MuRF3 results in a loss in expression of FHL2 and γ-filamin, whereas these proteins accumulate to abnormal levels in the hearts of mice lacking MuRF3. We conclude that MuRF3 controls the degradation of FHL2 and γ-filamin and is required for maintenance of ventricular integrity after MI.

Results

Generation of MuRF3 Mutant Mice. To examine the role of MuRF3 *in vivo*, we generated *MuRF3* mutant mice by replacing exon 4 of the *MuRF3* gene with a neomycin cassette and deleting the first coiled-coil domain of MuRF3 (Fig. 1*A*). Homozygous mutant *MuRF3* ($MuRF3^{-/-}$) mice were born in expected Mendelian ratios from $MuRF3^{+/-}$ intercrosses and had normal life spans and no overt abnormalities. RT-PCR using primers spanning the deleted region of the gene indicated that the deletion mutation eliminated nearly all detectable MuRF3 mRNA downstream of the neomycin insertion [supporting information (SI) Fig. 6 *A* and *B*]. Sequencing of the trace products of RT-PCR obtained from hearts of $MuRF3^{-/-}$ mice confirmed the absence of the fourth exon and showed that exon 3 was spliced in frame to exon 5. This mutant transcript was present at a level at least 20-fold less than that of the WT transcript. Therefore, we consider the *MuRF3* mutation to be comparable to a null allele, but we cannot rule out the possibility that the trace level of mutant transcript encodes a protein with residual function. The levels of expression of MuRF1 and MuRF2 transcripts were comparable in the hearts of WT and $MuRF3^{-/-}$ mice, indicating

Author contributions: J.F., J.A.S., R.v.d.N., and S.B. performed research; J.M.S., R.v.d.N., L.d.W., and J.A.R. contributed new reagents/analytic tools; J.F., E.v.R., J.A.S., J.M.S., S.L., J.A.R., R.B.-D., and E.N.O. analyzed data; and J.F., R.B.-D., and E.N.O. wrote the paper.

The authors declare no conflict of interest.

Abbreviation: MI, myocardial infarction.

¶To whom correspondence should be addressed. E-mail: eric.olson@utsouthwestern.edu.

This article contains supporting information online at www.pnas.org/cgi/content/full/0611726104/DC1.

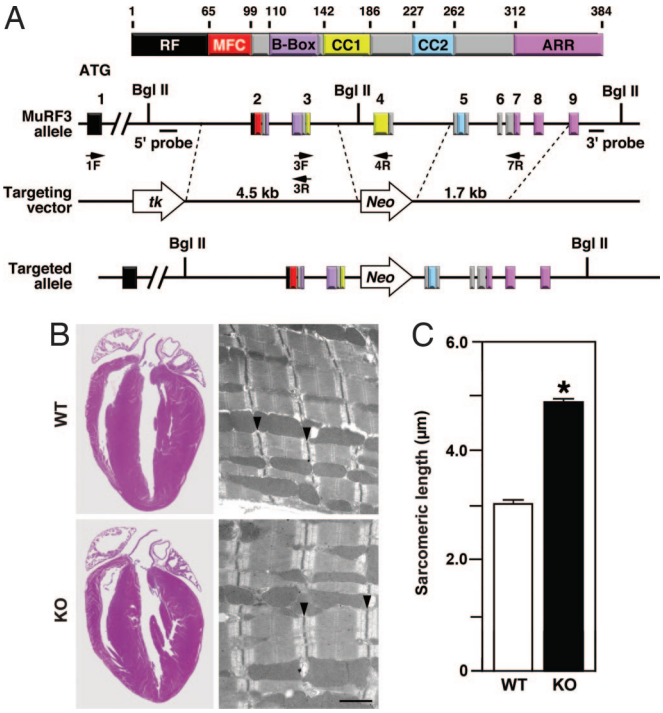

Fig. 1. Gene targeting and generation of *MuRF3* knockout mice. (*A*) Domains of mouse MuRF3 protein are shown at the top. RF, RING finger; MFC, MuRF family conserved domain; cc, coiled-coil; ARR, acidic-rich region. Amino acids are shown above the protein structure. The targeting vector contained a 4.5-kb 5′ arm, a 1.7-kb 3′ arm, a neomycin cassette (*Neo*), and a thymidine kinase gene (*tk*). Exons 1–9 are shown in boxes. Positions of 5′ and 3′ probes and PCR primers are indicated. (*B*) H&E-stained sections of 8-week-old WT and *MuRF3*$^{-/-}$ (KO) hearts. (*Right*) Representative sarcomeric structures visualized by transmission electron microscopy. (×6,000 magnification; scale bar, 2 μm.) (*C*) The distance between sarcomeric Z-lines in cardiomyocytes from WT and *MuRF3*$^{-/-}$ (KO) hearts as visualized by electron microscopy. Arrows indicate Z-lines. *, $P < 0.01$ vs. WT.

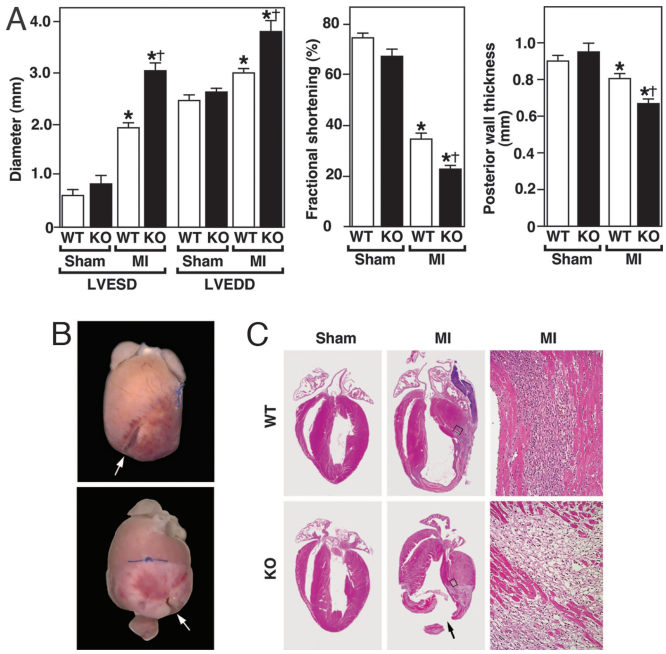

Fig. 2. Analyses of *MuRF3*$^{-/-}$ hearts. (*A*) Echocardiographic measurements of WT sham ($n = 10$), WT MI ($n = 12$), *MuRF3*$^{-/-}$ (KO) sham ($n = 7$), and KO MI ($n = 12$) mice. LVESD, left ventricular end-systolic dimension; LVEDD, left ventricular end-diastolic dimension. (*B*) Representative *MuRF3*$^{-/-}$ ruptured hearts 3 days after MI. Arrow indicates site of rupture. (*C*) H&E-stained sections of WT and *MuRF3*$^{-/-}$ (KO) hearts after sham operation or MI. Arrow indicates site of rupture. (*Right*) High-magnification images of the periinfarct zone (marked by box in *Center*). *, $P < 0.01$ vs. sham; †, $P < 0.01$ vs. WT MI.

that they were not up-regulated as a compensatory mechanism (data not shown).

The hearts of *MuRF3*$^{-/-}$ mice were the same size as WT, and histological analysis showed no morphological defects or signs of fibrosis (Fig. 1*B*). However, electron microscopy showed a significant increase in the distance between Z-discs, suggesting perturbation of the cardiac sarcomere (Fig. 1 *B* and *C*). Echocardiography showed no significant abnormality in fractional shortening, but a slight reduction in heart rate of the *MuRF3*$^{-/-}$ mice compared with WT littermates (Fig. 2*A* and data not shown).

Increased Mortality of *MuRF3*$^{-/-}$ Mice After MI. In light of the localization of MuRF3 to the sarcomere (14, 15), as well as its ability to stabilize microtubules (7), we wondered whether MuRF3 might be required to maintain structural integrity of the heart under conditions of acute stress, as occurs after MI. We therefore subjected *MuRF3*$^{-/-}$ mice to surgical MI to test their response to a rapid increase of left ventricular wall stress. Two to 3 days after MI, *MuRF3*$^{-/-}$ mice were notably lethargic, a phenotype reminiscent of heart failure. Echocardiography, performed 3 days after MI, revealed a more pronounced increase in left ventricular end-diastolic and end-systolic diameters resulting in a substantial decrease in fractional shortening in *MuRF3*$^{-/-}$ mice compared with WT littermates (Fig. 2*A* and SI Fig. 7). A further reduction in the posterior wall thickness of the left ventricle was seen in *MuRF3*$^{-/-}$ mice (Fig. 2*A*). These findings suggest that *MuRF3*$^{-/-}$ mice develop a dilative cardiomyopathic phenotype in response to MI.

A significant increase in mortality of *MuRF3*$^{-/-}$ mice compared with WT littermates was found within 5 days after MI (Table 1). Most dramatically, 10 of 13 *MuRF3*$^{-/-}$ mice that died from MI did so because of cardiac rupture, accounting for 77% of deaths (Fig. 2*B*). MI did not cause cardiac rupture in any WT mice, nor did the sham operation cause any lethality (Table 1). Gross and histological examination of hearts of *MuRF3*$^{-/-}$ mice that died from MI showed cardiac rupture at the border zone between the intact myocardium and infarcted area (Fig. 2 *B* and *C*). The infarct sizes 5 days after MI, as measured by morphometry, were not significantly different in WT and *MuRF3*$^{-/-}$ mice, comprising 32% and 36% of the left ventricular free wall, respectively. The degree of cardiac hypertrophy in *MuRF3*$^{-/-}$ and WT mice after MI was also not different between the groups (data not shown).

MuRF3$^{-/-}$ hearts contained degenerative myofibers between the infarcted and noninfarcted myocardium (Fig. 2*C*), suggesting an increase in cell death. Using TUNEL assay, we found that the hearts of *MuRF3*$^{-/-}$ mice showed a 3-fold increase in apoptosis in the periinfarct zone compared with WT littermates after MI (data not shown). In addition, intramural hemorrhage in the

Table 1. Lethality and cardiac rupture of *MuRF3*$^{-/-}$ mice after MI

Condition	WT*	KO
Sham	0/10 (0)	0/13 (0)
MI	4/25 (0)	13/26 (10)

*Shown is the number of mice that died after sham operation or MI over the total number of mice in each group. Numbers in parentheses indicate numbers of mice with cardiac rupture.

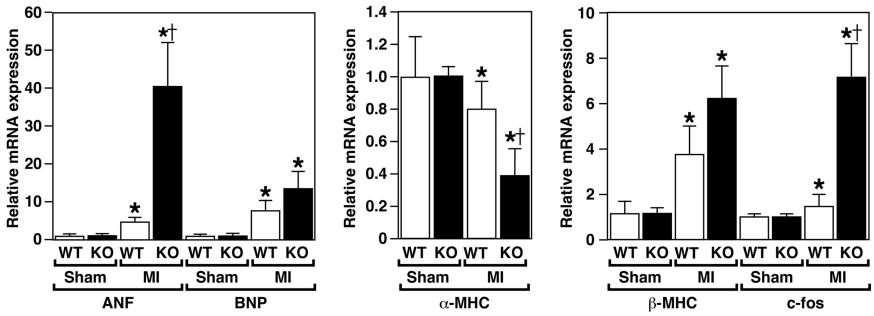

Fig. 3. Expression of cardiac stress markers. Real-time RT-PCR was used to measure the expression of transcripts encoding ANF, BNP, α-MHC, β-MHC, and c-fos in the hearts of WT sham ($n = 4$), WT MI ($n = 5$), *MuRF3*$^{-/-}$ (KO) sham ($n = 6$), and KO MI ($n = 6$) mice. *, $P < 0.01$ vs. sham; †, $P < 0.01$ vs. WT MI.

infarcted area was seen in *MuRF3*$^{-/-}$ mice but not in WT mice. Thus, the absence of MuRF3 rendered the heart highly susceptible to rupture in response to MI.

Up-Regulation of Cardiac Stress Markers in *MuRF3*$^{-/-}$ Mice. To assess the degree of cardiac stress resulting from MI, expression of the fetal gene program was measured within the noninfarcted interventricular septum. After MI, mRNA transcripts of the cardiac stress marker *atrial natriuretic factor* (*ANF*) and the immediate early gene *c-fos* were up-regulated more dramatically in *MuRF3*$^{-/-}$ mice compared with WT littermates, whereas transcripts encoding B-type natriuretic peptide (BNP) and β-myosin heavy chain, also markers of cardiac stress, showed similar regulation irrespective of genotype (Fig. 3). Transcripts encoding α-myosin heavy chain (α-MHC), which are typically down-regulated in response to cardiac stress, showed an exacerbated down-regulation in *MuRF3*$^{-/-}$ mice compared with WT mice (Fig. 3). The enhanced changes in the fetal gene program suggest a more severe degree of cardiac stress and heart failure in *MuRF3*$^{-/-}$ compared with WT animals after MI.

Reduced Cardiac Performance of *MuRF3*$^{-/-}$ Mice After Isoproterenol Administration. We also examined whether *MuRF3*$^{-/-}$ hearts displayed a reduction of cardiac function upon chronic administration of the β-adrenergic agonist isoproterenol, a well established inducer of cardiomyocyte apoptosis (16). Continuous isoproterenol infusion for 7 days resulted in a 45% increase in cardiac mass in WT mice versus a 32% increase in *MuRF3*$^{-/-}$ mice (Fig. 4*A* and SI Fig. 8*A*). Echocardiography showed a reduction in fractional shortening in mutant but not in WT mice after isoproterenol infusion (Fig. 4*B*). Mutant mice also showed a greater increase of the left ventricular end-systolic diameter compared with control littermates (SI Fig. 8*B*). TUNEL assays showed 2-fold more apoptosis in *MuRF3*$^{-/-}$ mice compared with WT mice treated with isoproterenol (Fig. 4*C*). These results further suggest that the absence of MuRF3 renders the heart susceptible to apoptosis after cardiac stress.

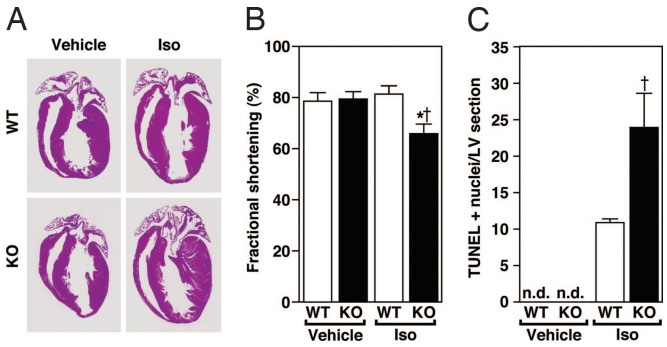

Fig. 4. Treatment of *MuRF3*$^{-/-}$ mice with isoproterenol reduces cardiac performance. (*A*) Representative H&E-stained sections of hearts from WT and *MuRF3*$^{-/-}$ (KO) mice treated with vehicle or isoproterenol (Iso) for 7 days. (*B*) Fractional shortening measured by echocardiography from WT vehicle-treated ($n = 5$), WT Iso-treated ($n = 8$), *MuRF3*$^{-/-}$ (KO) vehicle-treated ($n = 4$), and KO Iso-treated ($n = 8$) mice. (*C*) Numbers of TUNEL-positive nuclei per left ventricular section of WT vehicle-treated ($n = 2$), WT Iso-treated ($n = 3$), *MuRF3*$^{-/-}$ (KO) vehicle-treated ($n = 2$), and KO Iso-treated ($n = 3$) mice. n.d., none detected. *, $P < 0.01$ vs. sham; †, $P < 0.01$ vs. WT Iso.

MuRF3 Interacts with FHL2 and γ-Filamin. To begin to investigate the mechanism whereby MuRF3 maintains structural integrity of the heart, we sought to identify MuRF3 interaction partners in muscle cells by a yeast two-hybrid screen of a human heart cDNA library with MuRF3 as bait. Among the MuRF3-interacting proteins, we identified multiple clones encoding the intracellular adaptor protein FHL2 and γ-filamin (SI Fig. 9 *A* and *B*); their binding to MuRF3 was confirmed by coimmunoprecipitation experiments (Fig. 5 *A* and *B*). Specificity of MuRF3 binding was demonstrated by association of MuRF3 with γ-filamin but not α-filamin, which were expressed at comparable levels (data not shown) and which share 74% homology (Fig. 5*B*).

Deletion of the first coil-coiled domain of MuRF3 eliminated binding to both γ-filamin (data not shown) and FHL2 (Fig. 5*A*). The interaction of Myc-tagged MuRF3 with FHL2 and γ-filamin was readily detectable by coimmunoprecipitation. However, when non-epitope-tagged MuRF3 was overexpressed with FHL2 and γ-filamin in myoblasts, FHL2 and γ-filamin proteins failed to accumulate, suggesting that they are targets for MuRF3-dependent degradation (Fig. 5*C*). Because the Myc-tagged form of MuRF3 did not promote the degradation of FHL2 or γ-filamin, we believe that the epitope tag at the N terminus disrupts the function of the adjacent RING-finger domain.

FHL2 and γ-Filamin Accumulate Within *MuRF3*$^{-/-}$ Hearts. FHL2 and γ-filamin protein expression levels were measured in protein lysates of WT and *MuRF3*$^{-/-}$ hearts (Fig. 5*D*). FHL2 showed a slight but reproducible increase in expression, and γ-filamin showed a 5-fold increase in expression in *MuRF3*$^{-/-}$ hearts, suggesting that MuRF3 enhances their degradation *in vivo*. In contrast, mRNA expression levels of FHL2 and γ-filamin showed no difference in the hearts of *MuRF3*$^{-/-}$ and WT mice, suggesting that the accumulation of FHL2 and γ-filamin was due to reduced protein degradation and not an increase in gene expression (Fig. 5*E*).

Discussion

The results of this study show that MuRF3, a muscle-specific E3 ubiquitin ligase, is essential for maintenance of cardiac integrity and function after MI. MuRF3 associates with and appears to enhance degradation of FHL2 and γ-filamin, and the lack of

CELL BIOLOGY

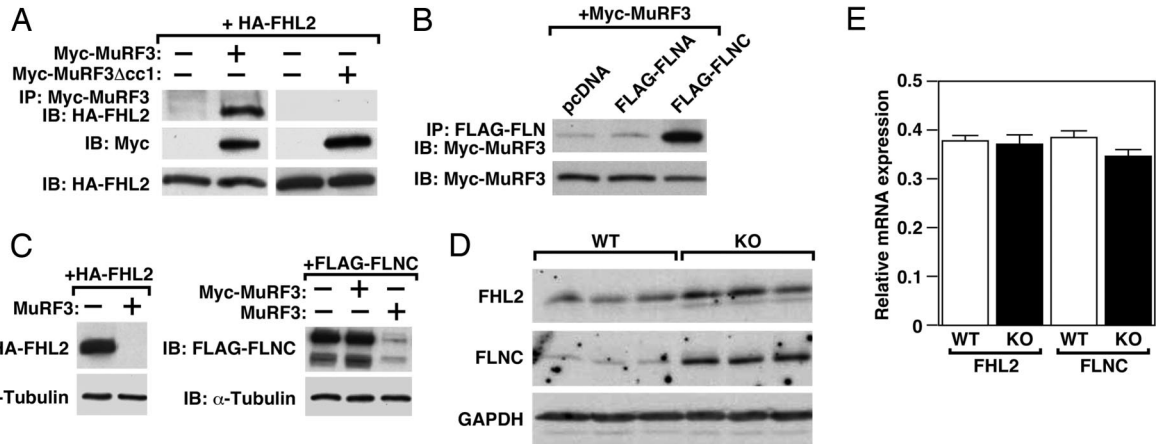

Fig. 5. MuRF3 interacts with and degrades FHL2 and γ-filamin. C2C12 cells were cotransfected with expression plasmids encoding Myc-MuRF3 or Myc-MuRF3Δcc1 and HA-FHL2 (*A*) or Flag-filamin A (Flag-FLNA) or Flag-γ-filamin (Flag-FLNC) (*B*) and coimmunoprecipitated 24 h posttransfection by using Myc or Flag antibody and immunoblotted with HA or Myc antibody. IP, immunoprecipitated; IB, immunoblotted. (*C*) C2C12 cells were cotransfected with expression plasmids encoding HA-FHL2 or Flag-γ-filamin (Flag-FLNC) with or without Myc-tagged or nontagged MuRF3. Protein lysates were used in Western blot analyses with HA or Flag antibody. α-Tubulin was used as control. (*D*) Endogenous FHL2 and γ-filamin (FLNC) proteins were measured in extracts from hearts of three individual WT and *MuRF3*$^{-/-}$ (KO) mice by using FHL2 and γ-filamin-specific antibodies. GAPDH was used as a control. (*E*) FHL2 and γ-filamin mRNA were measured by quantitative real-time PCR using ABI TaqMan probes and normalized to GAPDH. No change in mRNA expression of FHL2 and γ-filamin was found between WT ($n = 4$) and *MuRF3*$^{-/-}$ (KO, $n = 4$) mice hearts.

MuRF3 results in accumulation of these proteins, widening of the sarcomere, diminished cardiac contractility, and susceptibility to ventricular rupture. Given the association of MuRF proteins with the sarcomere (14, 15), their ability to bind and stabilize microtubules (7), and their E3 ligase activity (13), the susceptibility of *MuRF3*$^{-/-}$ mice to cardiac rupture could reflect structural and/or enzymatic functions of MuRF3.

Potential Causes of Cardiac Rupture in *MuRF3*$^{-/-}$ Mice. Abnormalities in protein degradation have recently been recognized as an important cause of cardiomyopathy and heart disease (1). E3 ubiquitin ligases play a key role in the control of protein degradation by providing specificity and efficiency to ubiquitination. To date, relatively few E3 ligases have been implicated in the degradation of myocardial proteins. Atrogin-1, an F-box protein, mediates myofibrillar protein degradation and can prevent calcineurin-mediated cardiac hypertrophy (17). MuRF1 mediates degradation of troponin I and, when overexpressed, reduces cardiomyocyte contractility (13). MuRF1 has also been reported to prevent cardiomyocyte hypertrophy in response to protein kinase Cε activation (18).

Our results identify FHL2 and γ-filamin as interaction partners of MuRF3; their degradation when coexpressed with MuRF3 and accumulation in the hearts of *MuRF3*$^{-/-}$ mice also implicate them as *in vivo* targets of MuRF3 and suggest a potential role in cardiac rupture. How the enhanced expression of FHL2 and γ-filamin might contribute to a loss of ventricular integrity, however, is less clear. Like MuRF proteins, FHL2 interacts with the M-band portion of titin and has been described as an adaptor for the compartmentalization of metabolic enzymes to sites of high energy consumption in the sarcomere (19) as well as an adaptor in numerous signaling and transcriptional pathways (20–22). Filamins act as actin-cross-linking proteins and participate in multiple cellular processes, including cell–cell and cell matrix connections, mechanoprotection, and various signaling networks (23). γ-filamin localizes to the Z-discs of the sarcomere, where it interacts with calsarcin/myozenin (24, 25) and myotilin (26), as well as to the muscle sarcolemma where it associates with δ- and γ-sarcoglycan (26, 27). A dominant form of myofibrillar myopathy has been ascribed to a mutation in the *FLNC* gene that results in γ-filamin aggregates, altered distribution of myotilin and the dystrophin–sarcoglycan complex, and myofibrillar degeneration (28). Abnormal localization of γ-filamin has also been linked to human myopathies (41, 42). Although we favor the idea that MuRF3 is required to regulate precise levels of FHL2 and γ-filamin (and probably other components of the sarcomere) such that the absence of MuRF3 sensitizes the heart to stress signals due to aberrant structure and function of the sarcomere, we cannot be certain that the accumulation of FHL2 and γ-filamin in *MuRF3*$^{-/-}$ hearts is responsible for cardiac rupture or hypersensitivity to isoproterenol administration.

Other Influences on Cardiac Rupture. MI leads to an immediate increase in cardiac wall stress and activates stress response mechanisms that aim to maintain the integrity of the ventricular wall. Although the molecular mechanisms leading to cardiac rupture after MI remain poorly understood, hypertension, diabetes, cardiac hypertrophy, and use of nonsteroidal antiinflammatory agents are considered as risk factors (29, 30). Mice lacking the angiotensin type 2 receptor (31), tissue-type plasminogen activator, urokinase receptor, or metalloelastase are also susceptible to cardiac rupture (32), whereas overexpression of FrzA/sFRP-1, a secreted antagonist of the Wnt/Frizzled pathway (33), and targeted deletion of matrix metalloproteinase-2 (34) and urokinase-type plasminogen activator (32) prevent cardiac rupture in mice after MI. In contrast to MuRF3, these mediators of inflammation and proteolysis are not muscle-specific and may act through different mechanisms than MuRF3 to modulate the response of the heart to acute stress.

Modulation of Muscle Structure and Function by MuRFs. Our finding that MuRF3 is required to maintain cardiac function after MI appears contradictory to studies showing that mice lacking MuRF1 and MAFbx, a SCF complex E3 ligase, were protected from skeletal muscle atrophy (8). Based on those findings, it was concluded that MuRF1 and MAFbx were involved in turnover of structural proteins, such that the absence of MuRF1 and MAFbx prevented skeletal muscle atrophy (8). However, no targets of MuRF1 were identified, and the cardiac phenotype of *MuRF1*$^{-/-}$ mice was not described, so it remains to be deter-

mined whether the *MuRF1*$^{-/-}$ heart is functionally compromised under conditions of cardiac stress.

MuRF1, -2, and -3 all localize to the M-line and Z-disk (7, 14, 15) and form heterodimers (14), raising the possibility that the phenotype of MuRF3 mutant mice may reveal only a subset of MuRF3 functions due to redundancy among MuRF proteins. Further analysis of the functions of MuRF proteins *in vivo* and of the consequences of compound *MuRF* gene deletion should reveal additional functions for this family of proteins in cardiac, as well as skeletal, muscle. The identification of additional partners and substrates or MuRF proteins also promises to provide further insights into the contributions of protein turnover to cardiac disease, as well as to offer new therapeutic targets for modification of cardiac function.

Materials and Methods

Generation of *MuRF3* Knockout Mice. The *MuRF3* targeting vector contained a 4.5-kb 5′ arm containing exons 2–3 and a 1.7-kb 3′ arm containing exons 5–8 of the mouse *MuRF3* gene. Exon 4, encoding the first coiled-coil domain, was replaced with a neomycin-resistance cassette. Targeting of mouse embryonic stem cells, generation of mouse chimeras, Southern blot analysis, PCR genotyping of genomic DNA, and RT-PCR were performed as described in ref. 35 (primer sequences are shown in SI Table 2). *MuRF3* mutant mice were backcrossed to C57Bl6 background for at least six generations before further investigation.

Surgical Procedures. Myocardial infarction (MI) was performed in 6- to 8-week-old male WT ($n = 25$) and *MuRF3*$^{-/-}$ (KO, $n = 26$) mice by ligating the left anterior descending artery by a surgeon blinded to the genotype as described in refs. 36 and 37. A sham operation in which the left anterior descending artery was not ligated was performed in WT ($n = 10$) and KO ($n = 13$) mice. Isoproterenol treatment and echocardiography were performed as described in refs. 36 and 37. See *SI Materials and Methods* for details. All animal experimental procedures were reviewed and approved by the institutional animal care and use committees of the University of Texas Southwestern Medical Center.

Histology, TUNEL, and Electron Microscopy. Histology, H&E staining, measurement of infarct size, TUNEL assay, and electron microscopy were performed as described in refs. 36 and 38. See *SI Materials and Methods* for details.

Cell Culture, Transfection, and Coimmunoprecipitation. Cell-culture and transfection experiments were performed in C2C12 cells by using Lipofectamine and Plus reagent (Invitrogen). Expression plasmids encoding tagged MuRF3 and Flag-γ-filamin are described in refs. 7 and 25, and HA-FHL2 was a gift from Daniel Garry (University of Texas Southwestern Medical Center). Coimmunoprecipitation (37) and Western blot analysis (39) were performed as previously described. See *SI Materials and Methods* for more details.

Yeast Two-Hybrid Screen. A human heart cDNA library encoding GAL4-transactivation domain fusion proteins (Invitrogen) was screened with a GAL4-MuRF3 bait in the yeast two-hybrid system, and positive clones were subjected to specificity tests as described in ref. 40.

RNA Isolation, Reverse Transcription, and Real-Time PCR. Total RNA was isolated from the noninfarcted part of the interventricular septum by using TRIzol reagent, and reverse transcription with SuperScript RNase H reverse transcriptase (both from Invitrogen) were performed as described in ref. 39. Real-time PCR was performed with TaqMan assays from Applied Biosystems probes by using the ABI 7000 real-time PCR instrument.

Statistical Methods. Values are presented as mean ± SEM. Gene expression was normalized to GAPDH mRNA and calculated as fold change over the respective sham-treated group. Differences in morphologic and biochemical parameters between groups were analyzed by Mann–Whitney *U* test or two-sided Student's *t* test. Statistics were calculated with Excel and SPSS software. A P value of <0.05 was considered to be statistically significant.

We thank J. Hill, T. McKinsey, and O. Nakagawa for insightful comments on the manuscript; D. Bellotto for help with electron microscopy; A. Tizenor and A. Diehl for help with graphics; J. Brown for editorial assistance; and I. Rybkin, K. Song, and J. Backs for helpful discussions. E.N.O. is supported by grants from the National Institutes of Health, the D. W. Reynolds Center for Clinical Cardiovascular Research, and the Robert A. Welch Foundation. J.F. was supported by a fellowship from Muscular Dystrophy Association and the Pfizer fellowship of the German Society of Cardiology.

1. Wang X, Robbins J (2006) *Circ Res* 99:1315–1328.
2. Ciechanover A (2006) *Neurology* 66:S7–S19.
3. Razeghi P, Sharma S, Ying J, Li YP, Stepkowski S, Reid MB, Taegtmeyer H (2003) *Circulation* 108:2536–2541.
4. Glass DJ (2003) *Nat Cell Biol* 5:87–90.
5. Depre C, Wang Q, Yan L, Hedhli N, Peter P, Chen L, Hong C, Hittinger L, Ghaleb B, Sadoshima J, *et al.* (2006) *Circulation* 114:1821–1828.
6. Powell SR (2006) *Am J Physiol* 291:H1–H19.
7. Spencer JA, Eliazer S, Ilaria RL, Jr, Richardson JA, Olson EN (2000) *J Cell Biol* 150:771–784.
8. Bodine SC, Latres E, Baumhueter S, Lai VK, Nunez L, Clarke BA, Poueymirou WT, Panaro FJ, Na E, Dharmarajan K, *et al.* (2001) *Science* 294:1704–1708.
9. Witt SH, Granzier H, Witt CC, Labeit S (2005) *J Mol Biol* 350:713–722.
10. McElhinny AS, Kakinuma K, Sorimachi H, Labeit S, Gregorio CC (2002) *J Cell Biol* 157:125–136.
11. Gotthardt M, Hammer RE, Hubner N, Monti J, Witt CC, McNabb M, Richardson JA, Granzier H, Labeit S, Herz J (2003) *J Biol Chem* 278:6059–6065.
12. Lange S, Xiang F, Yakovenko A, Vihola A, Hackman P, Rostkova E, Kristensen J, Brandmeier B, Franzen G, Hedberg B, *et al.* (2005) *Science* 308:1599–1603.
13. Kedar V, McDonough H, Arya R, Li HH, Rockman HA, Patterson C (2004) *Proc Natl Acad Sci USA* 101:18135–18140.
14. Centner T, Yano J, Kimura E, McElhinny AS, Pelin K, Witt CC, Bang ML, Trombitas K, Granzier H, Gregorio CC, *et al.* (2001) *J Mol Biol* 306:717–726.
15. McElhinny AS, Perry CN, Witt CC, Labeit S, Gregorio CC (2004) *J Cell Sci* 117:3175–3188.
16. Saito S, Hiroi Y, Zou Y, Aikawa R, Toko H, Shibasaki F, Yazaki Y, Nagai R, Komuro I (2000) *J Biol Chem* 275:34528–34533.
17. Li HH, Kedar V, Zhang C, McDonough H, Arya R, Wang DZ, Patterson C (2004) *J Clin Invest* 114:1058–1071.
18. Arya R, Kedar V, Hwang JR, McDonough H, Li HH, Taylor J, Patterson C (2004) *J Cell Biol* 167:1147–1159.
19. Lange S, Auerbach D, McLoughlin P, Perriard E, Schafer BW, Perriard JC, Ehler E (2002) *J Cell Sci* 115:4925–4936.
20. Samson T, Smyth N, Janetzky S, Wendler O, Muller JM, Schule R, von der Mark H, von der Mark K, Wixler V (2004) *J Biol Chem* 279:28641–28652.
21. Sun J, Yan G, Ren A, You B, Liao JK (2006) *Circ Res* 99:468–476.
22. Johannessen M, Moller S, Hansen T, Moens U, Van Ghelue M (2006) *Cell Mol Life Sci* 63:268–284.
23. Feng Y, Walsh CA (2004) *Nat Cell Biol* 6:1034–1038.
24. Faulkner G, Pallavicini A, Comelli A, Salamon M, Bortoletto G, Ievolella C, Trevisan S, Kojic S, Dalla Vecchia F, Laveder P, *et al.* (2000) *J Biol Chem* 275:41234–41242.
25. Frey N, Olson EN (2002) *J Biol Chem* 277:13998–14004.
26. van der Ven PF, Wiesner S, Salmikangas P, Auerbach D, Himmel M, Kempa S, Hayess K, Pacholsky D, Taivainen A, Schroder R, *et al.* (2000) *J Cell Biol* 151:235–248.
27. Thompson TG, Chan YM, Hack AA, Brosius M, Rajala M, Lidov HG, McNally EM, Watkins S, Kunkel LM (2000) *J Cell Biol* 148:115–126.
28. Vorgerd M, van der Ven PF, Bruchertseifer V, Lowe T, Kley RA, Schroder R, Lochmuller H, Himmel M, Koehler K, Furst DO, Huebner A (2005) *Am J Hum Genet* 77:297–304.
29. Bulkley BH, Roberts WC (1974) *Am J Med* 56:244–250.
30. Jugdutt BI, Basualdo CA (1989) *Can J Cardiol* 5:211–221.
31. Ichihara S, Senbonmatsu T, Price E, Jr, Ichiki T, Gaffney FA, Inagami T (2002) *Circulation* 106:2244–2249.

32. Heymans S, Luttun A, Nuyens D, Theilmeier G, Creemers E, Moons L, Dyspersin GD, Cleutjens JP, Shipley M, Angellilo A, *et al.* (1999) *Nat Med* 5:1135–1142.
33. Barandon L, Couffinhal T, Ezan J, Dufourcq P, Costet P, Alzieu P, Leroux L, Moreau C, Dare D, Duplaa C (2003) *Circulation* 108:2282–2289.
34. Matsumura S, Iwanaga S, Mochizuki S, Okamoto H, Ogawa S, Okada Y (2005) *J Clin Invest* 115:599–609.
35. Frey N, Barrientos T, Shelton JM, Frank D, Rutten H, Gehring D, Kuhn C, Lutz M, Rothermel B, Bassel-Duby R, *et al.* (2004) *Nat Med* 10:1336–1343.
36. van Rooij E, Doevendans PA, Crijns HJ, Heeneman S, Lips DJ, van Bilsen M, Williams RS, Olson EN, Bassel-Duby R, Rothermel BA, De Windt LJ (2004) *Circ Res* 94:e18–e26.
37. Song K, Backs J, McAnally J, Qi X, Gerard RD, Richardson JA, Hill JA, Bassel-Duby R, Olson EN (2006) *Cell* 125:453–466.
38. Naya FJ, Black BL, Wu H, Bassel-Duby R, Richardson JA, Hill JA, Olson EN (2002) *Nat Med* 8:1303–1309.
39. Bush E, Fielitz J, Melvin L, Martinez-Arnold M, McKinsey TA, Plichta R, Olson EN (2004) *Proc Natl Acad Sci USA* 101:2870–2875.
40. McKinsey TA, Zhang CL, Olson EN (2000) *Proc Natl Acad Sci USA* 97:14400–14405.
41. Kudryashova E, Kudryashov D, Kramerova I, Spencer MJ (2005) *J Mol Biol* 354:413–424.
42. Kallijarvi J, Lahtinen U, Hamalainen R, Lipsanen-Nyman M, Palvimo JJ, Lehesjoki AE (2005) *Exp Cell Res* 308:146–155.